New Method for Magnetometers Based Orientation Estimation

Valérie Renaudin, Muhammad Haris Afzal, Gérard Lachapelle
Schulich School of Engineering
Position Location and Navigation (PLAN) Group
University of Calgary, 2500 University Drive N.W.
Calgary, Alberta, Canada, T2N 1N4

Abstract- **Low cost magnetometers can be used for estimating the orientation with respect to the magnetic North. Although magnetometers work very well in clean magnetic environments like in the outdoors, they are strongly influenced by magnetic perturbations produced by manmade infrastructure in the indoors. Calibration techniques exist that can be used to compensate for these perturbations only if they are constant and associated with the navigation platform itself. But in the indoors, these perturbations vary spatially and render the previously available calibration techniques useless. In this paper, we present a new calibration technique that can be used to compensate for the varying magnetic perturbations on the host platform with better accuracy. Based on this new calibration algorithm, magnetic heading is estimated using multiple magnetometers mounted in a special geometric arrangement. Results show that the new calibration technique and heading computation successfully estimate the cumulative effects of perturbations and gives a better orientation estimate as compared with previous work.**

Keywords: Magnetometer, calibration, indoor magnetic field, pedestrian navigation

I. INTRODUCTION

The Earth's magnetic field has been used for several millennia for navigation. One of the first magnetic compasses was invented by the Chinese thousands of years ago. For this invention, a bowl filled with water was used as a leveling platform and a magnetic lodestone was placed on a plate floating on the water surface [1]. Nowadays, thanks to the advancements in Integrated Circuit (IC) fabrication and sensor technology, magnetometers are miniaturized and integrated in handheld devices. Consequently, their use for pedestrian navigation experiences increasing interest.

In the outdoors, global navigation satellites systems (GNSS) provide sub-metre positioning solution and additional sensors are considered as primary or aiding tools. Indoors, the satellite coverage is not sufficient to provide an accurate position estimate, not to mention the other issues that radio signals encounter in these environments. Therefore micro electro mechanical sensors (MEMS), such as inertial sensors, become the primary source to derive navigation solutions. The heading of a pedestrian in motion can be computed with the readings of a triad of magnetometers. As illustrated in Fig. 1,

knowing the horizontal component of the Earth's magnetic field and the local declination, the geographical azimuth φ can be derived as follows:

$$\varphi = \tan^{-1}\left(\frac{h_y}{h_x}\right) \pm D. \qquad (1)$$

However indoor environments are harsh for Earth's magnetic field measurements. Manmade infrastructures produce magnetic interferences that add local anomalies to the observations. These perturbations introduce errors in the derived azimuth.

In this paper, first a novel calibration method for a single tri-axis magnetometer on a host platform is proposed. It estimates the complete error sources without any simplification regarding the effect of magnetic deviation on the host platform. Because calibration algorithms do not treat external magnetic perturbations, a multi-magnetometer platform has been designed and a new algorithm based on the multi-magnetometer measurements is proposed to estimate the walking heading. Constraints from the geometric proprieties of the platform are utilized to estimate the final heading.
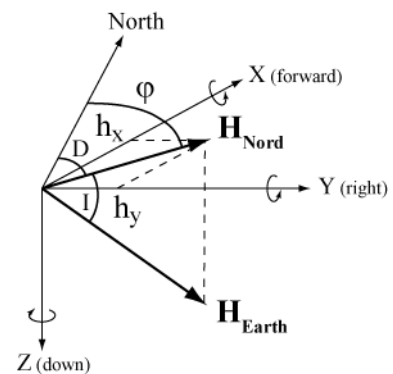

Figure 1. Earth's magnetic field in the sensor reference frame. The declination (D) is the angle between the geographic North and the horizontal component. The inclination (I) is the angle between the horizontal plane and the magnetic field vector.

This paper is organized into following sections. In section II, state of the art of existing magnetometer calibration techniques and processes to detect disturbances are reviewed. A magnetometer error analysis, detailed in section III, is used to derive the novel calibration algorithm in section IV. After applying the sensor's calibration to the multiple magnetometers of a new platform, their behavior becomes identical and hence they can be used together for estimating a more reliable heading. This is described in section V. The proposed solution is subject to specific constraints discussed in section VI. Finally, section VII presents the results of experimental tests for evaluating the validity of our solution.

II. STATE OF THE ART

Magnetic field distortions occur when the sensor is mounted on a platform introducing ferromagnetic elements in its vicinity. Calibration techniques to compensate for these unique magnetic characteristics of the host have already been proposed.

The compass swinging procedure [2] is a well-known calibration technique that requires leveling the platform and rotating it in a series of known headings. The two main limitations of this procedure are the need for external heading data and the constraint of leveling the platform. Another calibration technique in the magnetic domain consists of iterative batch least-squares (LS) [3] for estimating the deviation and combined scale factors of the magnetic readings. A non linear two step batch LS method using a change of variables provides the initial conditions. The shortcomings of this calibration lay in the assumptions that misalignments are negligible and that soft iron affects only the field on the sensor's axis aligned with the induced magnetic field. A geometric approach using an iterative Maximum Likelihood Estimator (MLE) [4] has also been proposed to best fit the onboard magnetometer's readings to an ellipsoid manifold during the rotation of the platform. A closed form optimal algorithm complements the process to compute the alignment matrix.

Beyond calibration techniques, some methods try to detect the perturbations and compensate for them. They rely on using redundant and complementary sensors. In [5], an Extended Kalman Filter estimates the heading with a gyro-aiding compass. Once interferences are detected, the measurement noise covariance matrix is adapted accordingly. Adaptive techniques are very sensitive to the covariance of the estimation algorithm and may lead to misinterpretation of magnetic perturbations. Finally in [6], readings from a two axis magnetometer mounted on a robot doing quick rotation are used to detect and evaluate magnetic distortions. This approach requires a high rotation speed and sampling rate.

III. MAGNETOMETER ERROR ANALYSIS

The main errors of a magnetometer are the scale factor, sensor offsets, sensor non-orthogonality, misalignments and magnetic deviation [7]. The first four errors are instrumentation errors whereas the magnetic deviation depends on the surrounding magnetic field anomalies. The following section examines each error in the sensor frame.

A. Instrumentation errors

Instrumentation errors are mainly due to fabrication limitations. They can be considered as unique and constant for one specific triad of magnetometers. Because the sensitivity of each sensing element of a triad may be different, constants of proportionality relating input to output on each axis have to be considered. The scale factor matrix $\mathbf{S}$ represents these unknowns:

$$\mathbf{S} = \mathrm{diag}\begin{pmatrix} s_x & s_y & s_z \end{pmatrix}. \qquad (2)$$

Ideally the axes of the triad are mounted perfectly aligned with the axes of the sensor and they are orthogonal between each other. Unfortunately due to fabrication issues, this may not be the case, introducing misalignment and non-orthogonality errors in the readings. Non-orthogonal sensing elements can be modeled with a matrix $\mathbf{N}$, where the column vectors give the direction of each sensor axis in the sensor frame. This matrix will also model misalignment errors, i.e. the rotation angles required to align the axes with the sensor frame. To correct for non-orthogonality and misalignment errors, we need to consider the matrix $\mathbf{M}$ corresponding to the inverse of $\mathbf{N}$. $\mathbf{M}$ can be modeled as

$$\mathbf{M} = \mathbf{N}^{-1} = \begin{bmatrix} \varepsilon_x & \varepsilon_y & \varepsilon_z \end{bmatrix}^{-1} \qquad (3)$$

where ε_x, ε_y and ε_z are vectors of size 3 that give respectively the directions of the sensor's x, y and z axes in the sensor frame.

Finally, the sensor offset introduces a bias $\mathbf{b_{so}}$ in the output. It is modeled as one bias per axis as

$$\mathbf{b_{so}} = \begin{bmatrix} b_{so_z} & b_{so_y} & b_{so_z} \end{bmatrix}^{\mathrm{T}}. \qquad (4)$$

B. Magnetic deviation

Errors in sensing the Earth's magnetic field come from the local deviation of the magnetic vector due to onboard hardware and surrounding magnetic materials. The magnetization characteristics of the sensor are almost linear and consist of soft iron and hard iron parts [8].

The soft component of the magnetic deviation corresponds to induced magnetization caused by the permeability of ferromagnetic compounds interacting with an external field. It changes the field sensors both in intensity and direction. Soft iron effect can be modeled as a 3 by 3 matrix as follows:

$$\mathbf{A_{si}} = \begin{bmatrix} a_{11} & a_{12} & a_{13} \\ a_{12} & a_{22} & a_{23} \\ a_{13} & a_{32} & a_{33} \end{bmatrix}. \qquad (5)$$

It is worth mentioning that no simplification is made on this matrix in order to ease the calibration estimation, for example eliminating the non diagonal components, which was done in previous work.

The hard component of the magnetic deviation corresponds to a permanent magnetic deviation. It results from permanent magnets and magnetic hysteresis, i.e. remanence of magnetized iron materials. Its action is equivalent to the sensor offsets and can be modeled as a bias $\mathbf{b_{hi}}$:

$$\mathbf{b_{hi}} = \begin{bmatrix} b_{hi_x} & b_{hi_y} & b_{hi_z} \end{bmatrix}^T. \qquad (6)$$

C. Magnetometer error modeling

The complete error model for the triad of magnetometers combines both instrumentation errors and magnetic deviation. The following equation gives the complete model in the sensor frame:

$$\begin{aligned} \mathbf{\hat{h}} &= \mathbf{SM}\left(\mathbf{A_{si}h} - \mathbf{b_{hi}}\right) - \mathbf{b_{so}} + \mathbf{n} \\ &= \mathbf{SMA_{si}h} - \mathbf{SMb_{hi}} - \mathbf{b_{so}} + \mathbf{n} \qquad (7) \\ &= \mathbf{Ah} - \mathbf{b} + \mathbf{n} \end{aligned}$$

where $\mathbf{h}$ is the error free magnetic field in the sensor frame, $\mathbf{\hat{h}}$ are the readings from the triad of magnetometers in the sensor frame too and $\mathbf{n}$ is Gaussian wideband noise. $\mathbf{A} = \mathbf{SMA_{si}}$ is a 3 by 3 matrix combining scale factors, misalignments and soft iron disturbances. $\mathbf{b} = \mathbf{SMb_{hi}} + \mathbf{b_{so}}$ is the combined bias.

IV. PROPOSED ALGORITHM FOR MAGNETOMETER CALIBRATION

A. Geometric constraint on the measured magnetic field ellipsoid

While performing 360 degrees turns in space, with the sensor located in a perturbation free environment, the locus described by the readings of a triad of magnetometers should be a sphere with a radius equal to the magnitude of the local Earth's magnetic field [3]. This magnitude H_m can be extracted from a geomagnetic model [9]:

$$H_m^2 - \|\mathbf{h}\|^2 = H_m^2 - \mathbf{h}^T\mathbf{h} = 0. \qquad (8)$$

If the square transformation matrix $\mathbf{A}$ and the combined bias $\mathbf{b}$ are known, then (7) can be rewritten as

$$\mathbf{h} = \mathbf{A}^{-1}(\mathbf{\hat{h}} + \mathbf{b} - \mathbf{n}). \qquad (9)$$

Substituting (9) in (8) and then expanding, gives

$$\mathbf{\hat{h}}^T\mathbf{Q}\mathbf{\hat{h}} + 2\mathbf{b}^T\mathbf{Q}\mathbf{\hat{h}} + \mathbf{b}^T\mathbf{Q}\mathbf{b} - H_m^2 = 0. \qquad (10)$$

With $\mathbf{Q} = \left(\mathbf{A}^{-1}\right)^T \mathbf{A}^{-1}$, $\mathbf{u} = 2\,\mathbf{Q}^T\mathbf{b}$ and $k = \mathbf{b}^T\mathbf{Q}\mathbf{b} - H_m^2$, (10) becomes

$$\mathbf{\hat{h}}^T\mathbf{Q}\mathbf{\hat{h}} + \mathbf{u}^T\mathbf{\hat{h}} + k = 0. \qquad (11)$$

Equation (11) represents a general plane of the second order. It describes a surface, e.g. a hyperboloid, a cone or an ellipsoid. As $\mathbf{Q}$ is a positive definite matrix, based on [10], if the following condition holds then (11) describes an ellipsoid:

$$\mathbf{u}^T\mathbf{Q}^{-1}\mathbf{u} > 4k. \qquad (12)$$

Differencing the terms on the left and right sides of the inequality in (12) gives

$$\mathbf{u}^T\mathbf{Q}^{-1}\mathbf{u} - 4k = H_m^2. \qquad (13)$$

The amplitude of the Earth Magnetic field is strictly positive, therefore condition (12) holds and (11) describes an ellipsoid. Consequently calibrating the triad of magnetometers corresponds to finding the parameters of (11) knowing that this second order equation describes an ellipsoid.

B. Calibration algorithm

If it is possible to collect magnetic field readings along several orientations that best describe the ellipsoid in a perturbation free environment, then the constraint (8) can be used to calibrate the magnetometers on the host platform. To our knowledge, the proposed calibration algorithm is novel for two following main reasons.

- It does not require any assumption on the magnetic deviation (5).

- It calibrates directly the magnetic readings without estimating the geometrical proprieties of the ellipsoid (rotation, translation and lengths of the semi-axes).

The proposed calibration algorithm comprises two steps. First the parameters of the ellipsoid equation are estimated and then the calibration elements $\mathbf{A}$ and $\mathbf{b}$ of (7) are derived.

1) Estimation of the ellipsoid equation. Because we proved that (11) describes an ellipsoid, it is possible to exploit a constraint that is specific to this type of surface to estimate the parameters of the ellipsoid equation. This constraint relates the parameters $\mathbf{Q}$, $\mathbf{u}$ and k from (11). One interesting solution to solve for these parameters is to use the geometric approach in [11]. It solves a minimisation problem using Lagrange multiplier method.

2) Estimation of the calibration parameters. The next step consists in extracting the elements $\mathbf{A}$ and $\mathbf{b}$, defined in (7) and

required to calibrate the magnetometers data. From (11), one has

$$Q = \left(A^{-1}\right)^T A^{-1}, \qquad (14)$$

$$u = 2Q^T b, \qquad (15)$$

$$k = b^T Q b - H_m^2. \qquad (16)$$

The combined bias b, corresponding to the translation of the ellipsoid coordinate system, is therefore given by

$$b = \frac{1}{2}Q^{-1}u. \qquad (17)$$

Because Q is a positive definite matrix, an eigen-decomposition can be applied.

$$Q = \alpha V D V^T \qquad (18)$$

where $\alpha \in \mathbb{R}$, V corresponds to the eigenvectors of QQ^T and D is a 3x3 diagonal matrix containing the eigenvalues λ_i, $i \in \{1, 2, 3\}$. The columns of V form the basis vector directions for Q.

Let $\sqrt{D} = \begin{bmatrix} \sqrt{\lambda_1} & 0 & 0 \\ 0 & \sqrt{\lambda_2} & 0 \\ 0 & 0 & \sqrt{\lambda_3} \end{bmatrix}$ and $B = V\sqrt{\alpha D}V^T$. We can then write

$$B^T B = V\sqrt{\alpha D}V^T V\sqrt{\alpha D}V^T = \alpha V D V^T. \qquad (19)$$

B corresponds to the matrix square root of Q and gives the solution for A^{-1} in (14). To find α, we apply the constraint (16) on the norm of the magnetic field measurement. Expanding (11) while introducing (18) gives

$$\hat{h}^T V\alpha D V^T\hat{h} + 2b^T V\alpha D V\hat{h} + b^T V\alpha D V b - H_m^2 = 0. \qquad (20)$$

The introduction of α changes the definition of k and (16) becomes

$$k = b^T V D V b - \frac{H_m^2}{\alpha}. \qquad (21)$$

Expanding (21) using (17), it is possible to compute α as follows:

$$\alpha = \frac{4\,H_m^2}{4\,k - (V^T u)^T D^{-1}(V^T u)}. \qquad (22)$$

Finally (7) can be applied on the magnetic field measurements to calibrate for the host platform influence. Calibrated magnetic field measurements are given by

$$h = V\sqrt{\alpha D}\,V^T\,(\hat{h} + b). \qquad (23)$$

V. HEADING BASED ON A MULTI-MAGNETOMETER PLATFROM

If it would be possible to collect magnetic field readings along several orientations that best describe the ellipsoid at the same time, then we could apply the previous calibration algorithm to calibrate the host platform on the fly.

Following this idea, a multi-magnetometer platform has been designed. It contains 12 triads of magnetometers located on two perpendicular circles, as illustrated on Fig. 2. Each circle is composed of 6 triads whose horizontal axes [x, y] are coplanar and with 60 degrees angle difference between two x axes.

After performing individual calibration of each magnetometer using the algorithm explained in section IV, all the instrumentation as well as platform errors associated with the sensors are compensated for. Thus the output of each magnetometer triad will be the same 3D magnetic field at that particular location.

The ideal magnetic field in absence of any perturbation sources at a particular location and time can be estimated using one of the magnetic field models, e.g. CGRF [9].
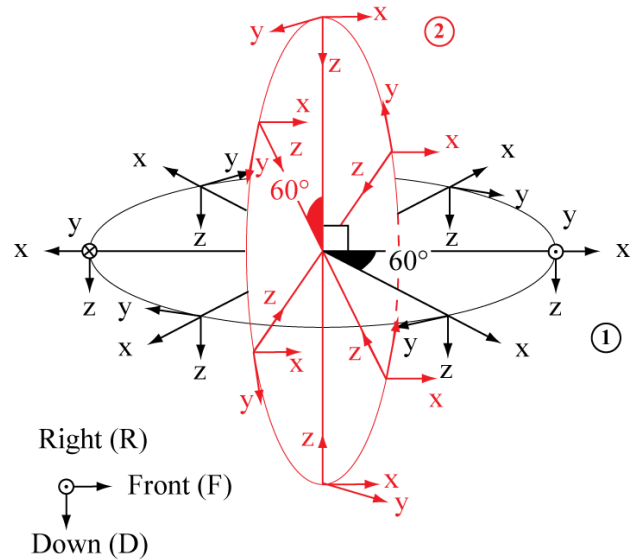

Figure 2. Multisensors magnetometers platform.
Each triad of magnetometers is represented by its three axes [x,y,z].
The platform frame is represented by the triad [F,R,D].

The amplitude of the magnetic field measured by any magnetometer triad at some particular instant is given by

$$H_m = \sqrt{h_x^2 + h_y^2 + h_z^2} \qquad (24)$$

where H_m is the total field intensity measured by a magnetometer triad and h_x , h_y , h_z are the field components respectively along the x, y and z axes of the sensor.

In presence of perturbations, this total field intensity will not correspond to the one predicted by the geomagnetic field model. Fig. 3 illustrates the effects of a perturbation source on the total intensity of the magnetic field.

This information can be utilized for compensating the magnetometer triads so as to bring the total measured magnetic field close to the predicted one. A LS estimation technique can be applied as follows, for this purpose.

1) Predict the total field intensity. This is achieved by utilizing one of the models like CGRF. Lets call it H_m .

2) Estimate the measured field intensity. This is computed by using (24).

3) Compute the field misclosure. From (24), the predicted field component can be computed as

$$\hat{h}_x^2 = H_m^2 - h_y^2 - h_z^2 . \qquad (25)$$

Then the misclosure will be given by

$$W = \hat{h}_x^2 - h_x^2 . \qquad (26)$$

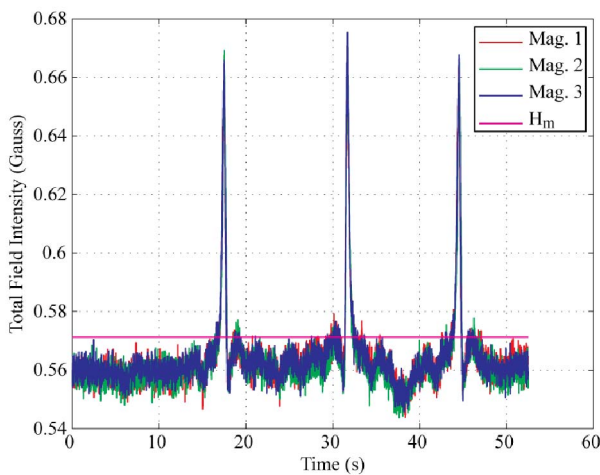*4) Jacobian matrix.* In this case, the jacobian comes out to be

Figure 3.   Effects of a perturbation on the measured magnetic field

$$J = 2\, h_x . \qquad (27)$$

5) Estimate the compensation for the field component. Now by solving the following LS equation, the compensation δ, required in one of the components, can be estimated.

$$\delta = \left(J^T P J\right)^{-1} J^T P W \qquad (28)$$

where P is the inverse covariance matrix. At the moment, the P matrix is not used.

6) Compensated heading. Applying steps 1 to 5 to all of the 12 magnetometers will compensate one of the components of each sensor so as to bring the measured total field close to the predicted one. This can also cause bias in the final heading computed using the compensated components. Due to the geometric arrangement of the platform, these biases if present, will be opposite for each opposite pair of sensors. Therefore by taking the mean of each set, comprising of sensors on opposite sides of a circle (see Fig. 2), this common but opposite bias can be compensated for. This gives us six heading estimates (one for each opposite set of sensor). Resolving these six heading estimates to the platform's frame and averaging them will reduce the overall noise level. Fig. 2 depicts the overall geometric arrangement of the 12 magnetometers on the platform. In this way, the geometric arrangement of the sensors is used to compensate for the heading estimate bias.

VI.   CONSTRAINTS ON THE MULTI-MAGNETOMETER PLATFORM

A.   Same error characteristics for all magnetometers

The new multi-magnetometer based heading estimation will work only under the constraint that all magnetometers have similar error characteristics. Otherwise, errors specific to each individual magnetometer should be considered and algorithm described in section V will no longer be valid. To assess this hypothesis H_1, an error analysis of all triads was conducted.

The multi-magnetometer platform consists of anisotropic magneto resistive (AMR) sensors HMC5843 from Honeywell. They are made of Permalloy thin films deposited on a silicon substrate in Wheatstone resistor bridge configuration. These sensors are affected by the instrumentation errors described in section III.A, plus cross-axis sensitivity. Indeed the sensitivity of AMR sensors may vary based on the field applied in the cross-axis direction, i.e. perpendicular to sensitive axis [8]. In geometric terms, the cross-axis sensed field can be considered as misalignment. It depends on applied field strength as well as AMR sensors fabrication. Magnetic hysteresis will also contribute to cross-axis sensitivity as AMR sensors tend to acquire different magnetizations in different regions within the sensor itself.

An advantage of AMR sensors is their immunity from turn on bias and changes in scale factor. This property allows us to calibrate all of the magnetometers individually and estimate these offsets and scale factors that can be used for the complete life span of the sensors [8]. This leaves us with the stochastic errors associated with each AMR sensor. In order for the hypothesis to hold, the stochastic errors associated with each magnetometer must have similar characteristics.

Allan variance analysis was applied to sixteen hours of data, recorded in static conditions. For the conciseness of the paper, results are presented only for two triads of magnetometers. Fig. 4 shows the Allan deviation plot for two triads of magnetometers. Wideband noise and bias instability are clearly visible on this plot. The Allan deviation analysis concludes that magnetometer data are contaminated by wideband noise for small cluster times and by a correlated noise representing a bias instability for large cluster times. It can also be observed that both magnetometers have nearly identical error characteristics. This observation is confirmed by the error values given in Table 1.

Although the noise characteristics of all the sensors are fairly similar, this does not mean that the sensors will behave in harmony based on their error characteristics. For example the drift associated with different sensors may be dissimilar causing them to behave differently. This is more dependent on the sensor type used. The multi-magnetometer platform used for this work is composed of AMR magnetic field sensors by Honeywell. These AMR sensors are known to have fairly stable error characteristics. In light of the noise characteristics modeling as well as the sensor type used, it can be concluded that hypothesis H_1 holds to some extent.

B. Uniform magnetic field on the platform

The proposed heading estimation algorithm holds only if all magnetometers from the multi-magnetometer platform sense the same magnetic field at the same time. Hence the hypothesis H_2 is that the local magnetic field is uniform in the vicinity of the multi-magnetometer platform.
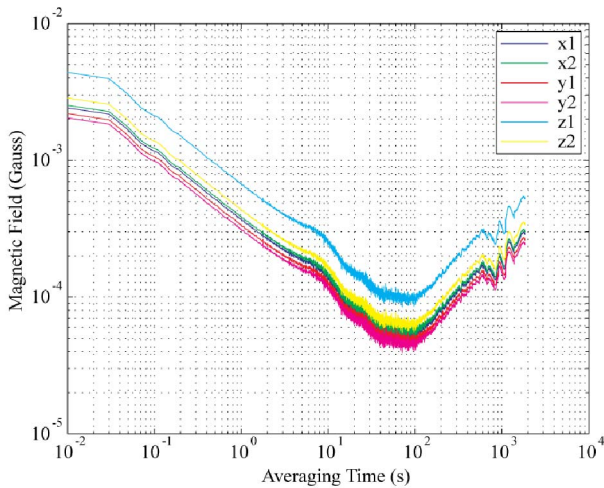

Figure 4.   Allan deviation plot for two tri-axes magnetometer with calibration coil usage.

TABLE I.   IDENTIFIED ERROR COEFFICIENTS FOR TWO TRIADS OF MAGNETOMETERS

Parameters	x axis		y axis		z axis	
Tri-axes magnetometer	*1*	*2*	*1*	*2*	*1*	*2*
Wideband noise PSD $\left(G{\times}10^4/\sqrt{Hz}\right)$	3.38	3.23	3.24	3.1	3.38	3.38
Bias PSD $\left(G{\times}10^5/\sqrt{Hz}\right)$	3.91	3.89	3.9	3.9	3.91	3.89
Correlation time (s)	70	71	70	69	70	70

The multi-magnetometer hardware senses the local magnetic field along several orientations at the same time. Because the measurements are done instantaneously, no time variation has to be considered. However spatial variations of the magnetic field in the vicinity of the multi-magnetometer platform will affect the proposed heading estimation.

Indoors, the sources of magnetic disturbances are numerous and their impact can hardly be modeled. Typical examples of perturbation's sources are elevators, wiring, building infrastructure and furniture.

Because the local magnetic perturbation is the sum of multiple disturbances generated by components usually non visible to the user, it is hardly possible to model them. Note that the use of a map of existing disturbances, pre-recorded in a calibration phase, could be a way to compensate for these errors. Still, a first approach consists in quantifying the contribution of a permanent magnet to the external magnetic field. If the permanent magnet is assumed to be equivalent to a magnetic dipole moment, then for distances bigger than the characteristic length of the dipole, the following equations approximate the external magnetic field in the dipole coordinate frame [8].

$$B_x = \frac{\mu_0 M}{4\pi}\left(\frac{3\cos^2\theta - 1}{d^3}\right)$$
$$B_y = \frac{\mu_0 M}{4\pi}\left(\frac{3\cos\theta\,\sin\theta}{d^3}\right) \tag{29}$$

where (B_x, B_y) are the magnetic field components measured at the distance d from the dipole. (x, y) represents the dipole's frame. θ is the angle between the dipole axis and the location of the magnetic field measurement. M is the strength of the dipole moment and μ_0 is the permeability constant. All parameters are depicted in Fig. 5.
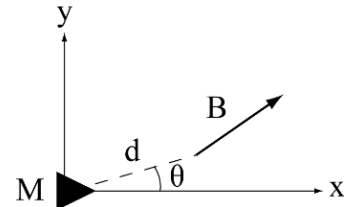

Figure 5.   External magnetic field **B** due to a magnetic dipole moment M in the dipole coordinate frame (x, y).

In (29), there is an inverse cubic law between the external magnetic field strength and the separation d. Therefore the impact of external magnetic sources is expected to drop off rapidly and become linear in the vicinity of the multi-magnetometer platform. Principally the separation between the multi-magnetometer platform and the perturbation sources plus the dimensions of the platform itself will impact the hypothesis H_2.

Experimental tests have been conducted to assess the impact of a permanent magnet on triads of magnetometers in a perturbation free environment. First results have shown that with a 1 meter separation from the magnet, not between sensors, differences between the various magnetometer readings were barely observable. This should be further investigated with different magnets and real indoor environments.

VII. EXPERIMENTAL ASSESSMENT OF THE PROPOSED ALGORITHMS

A. New calibration algorithm for the magnetometers on the host platform

Each HMC5843 tri-axis magnetometer from Honeywell, on the multi-magnetometer platform, has been calibrated using the algorithm described in section IV.B. Magnetic field measurements have been collected in a magnetic perturbation free sport court. The multi-magnetometer platform was turned in all directions, as depicted in Fig. 6.

To assess the performance of the new calibration algorithm, calibration results have been compared with the common iterative LS algorithm proposed in [3].

First, it is interesting to notice that [3] estimates only a part of the magnetometer error, because it assumes that the soft iron effect can be modeled as a diagonal matrix and that misalignments are negligible. In contrast, the novel algorithm calibrates all errors, i.e. both instrumentation errors and magnetic deviation effect, as it does not require any simplification of the error model.

For each magnetometer, 8795 readings have been used to compute the calibration parameters with both algorithms. Table 2 gives the calibration results obtained with both calibration algorithms for the triad number 1. For each sensor from the multi-magnetometer platform the following function has been evaluated with calibrated data.

$$f(\mathbf{A}^{*},\mathbf{b}^{*})=\sqrt{\left| H_m^2 - \left(\mathbf{A}^{*-1}(\hat{\mathbf{h}} + \mathbf{b}^{*}) \right)^{T} \left(\mathbf{A}^{*-1}(\hat{\mathbf{h}} + \mathbf{b}^{*}) \right) \right|}. \quad (30)$$

$\mathbf{A}^{*}$ and $\mathbf{b}^{*}$ correspond to optimal estimates of the calibration parameters defined in (7). H_m is given by the model [9] and equals to 0.57 Gauss in Calgary at the time of our experiment.

The mean error on the 12 magnetometer triads obtained with the iterative LS is 0.088 Gauss, while it is 6.9×10^{-9} Gauss with the novel algorithm. The difference between both errors is noticeable. The small error for the iterative LS suggests that, in this environment, the algorithm's assumptions hold. This can be explained by the fact that special care has been taken in the hardware design, as no metallic part has been used, and no magnetic perturbation is expected in the sport court.

Because indoor environments may induce magnetization on the platform and the novel algorithm should be able to estimate this effect, the algorithm has been tested on data collected in an office building, the Calgary Center for Innovative Technology (CCIT) at the University of Calgary. The experimental location is situated at the second floor of the building, in area corridor, where an induced magnetic deviation on the platform is expected. Table 3 provides the calibration outputs in this new location for the same sensor as used in the sport court. Fig. 7 and Fig. 8 illustrate the magnetic field measurements for three tri-axis magnetometers before and after the novel calibration respectively.

First it is interesting to observe that the calibration parameter values have changed between the two environments. The amplitude change of the combined bias $\mathbf{b}$ is in the noise level of the Honeywell sensor. No significant change in the hard iron effect was expected. However changes in the matrix $\mathbf{A}$, including the soft iron effect, are more significant. In this context, the novel algorithm provides better error modeling than the iterative LS.
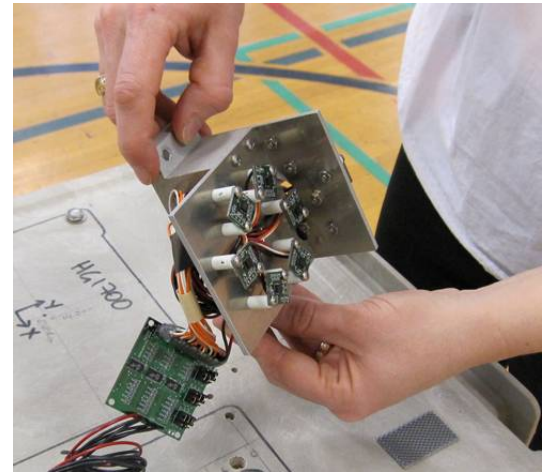

Figure 6. Data collection of magnetic field in space for the calibration of each triad of magnetometers

TABLE II. CALIBRATION PARAMETERS ESTIMATED WITH 2 DIFFERENT ALGORITHMS FOR THE TRI-AXES MAG. 1 IN THE SPORT COURT

Algorithm	New algorithm			iterative LS
b: combined bias [Gauss]	-0.059 0.203 -0.050			-0.054 0.202 -0.051
Scale factors and diagonal terms of soft iron [n.u.]	N/A			0.916 0.993 0.948
A: Scale factors, soft iron and misalignments [n.u.]	1.024 0.001 0.007	0.001 1.014 0.002	0.007 0.002 1.060	N/A

TABLE III. CALIBRATION PARAMETERS ESTIMATED WITH TWO DIFFERENT ALGORITHMS FOR THE TRI-AXES MAG. 1 IN THE CCIT BUILDING

Algorithm	new algorithm			iterative LS
b: Combined bias [Gauss]	-0.061			-0.068
	0.196			0.194
	-0.048			-0.051
Scale factors and diagonal terms of soft iron [n.u.]	N/A			1.022
				1.206
				1.137
A: Scale factors, soft iron and misalignments [n.u.]	0.870	0.003	0.007	N/A
	0.003	0.853	0.009	
	0.007	0.009	0.893	

The mean error, computed with (30), on the 12 triads of magnetometers gives 0.13 Gauss with the iterative LS, and 7×10^{-9} Gauss with the novel algorithm. It can be observed that the mean error has amplified by a factor of nearly 1.5 for the iterative LS between the sport court and the CCIT building, whereas the one from the novel algorithm remains in the same order. This confirms the fact that soft iron is better modeled with the second option. Furthermore proper calibration can even model partially the influence of surrounding magnetic elements through the soft iron on the platform itself.

B. Multi-magnetometer based heading estimation

After applying the calibration algorithm, an artificial perturbation source was created using a strong magnet. Then a trajectory was traversed over the perturbation source in the sport court (Fig. 9). As soon as the cart came in the vicinity of perturbation, a strong magnetic field was experienced by the sensors resulting in a false heading estimate. This was compensated for by utilizing the proposed multi-magnetometer heading estimator. Fig. 10 depicts the results of single magnetometer versus multi-magnetometer heading estimate. Table 4 summarizes the overall maximum errors of the two approaches.
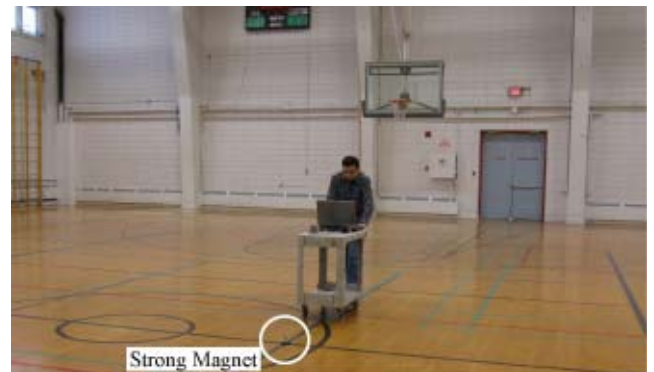

Figure 7. Uncalibrated magnetic field measurements in Gauss recorded in the CCIT building

Figure 9. Data collection with the multi-magnetometer platform, in a sport court, rolling over a strong magnet with a non mettalic cart.

Figure 8. Calibrated magnetic field measurements in Gauss recorded in the CCIT building
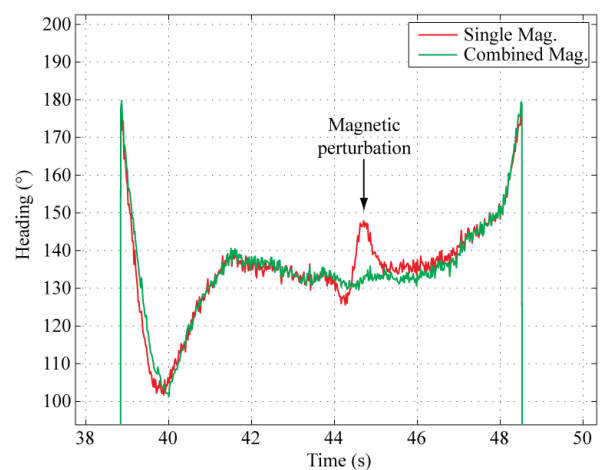

Figure 10. Heading estimates in presence of a perturbation source

TABLE IV. SINGLE VERSUS MULTIPLE MAGNETOMETER HEADING ERRORS IN PRESENCE OF A STRONG MAGNET

Heading Estimator	Max. Deflection
Single Magnetometer	16°
Multiple Magnetometer	4°

VIII. CONCLUSIONS

A novel calibration algorithm that deals with both instrumentation errors and magnetic deviation on the host platform has been proposed. Because it does not require any simplification on the error modeling, it overcomes the limitations of previous algorithms. Experimental results show that the performance of the algorithm supersedes that of the classical iterative LS calibration in the magnetic field domain.

A multi-magnetometer platform with twelve tri-axis magnetometers has been developed. The use of the geometric proprieties of this arrangement to estimate the walking direction is shown to have an advantage over a single triad of magnetometer. Heading estimated using multiple magnetometer arrangement gives much better results in perturbed environments and reduces the overall error in the heading's estimate by a factor of 4. Further developments based on this approach are being investigated.

REFERENCES

[1] A.A. Kaufman, R.O. Hansen and Robert L.K. Kleinberg, Principles of the magnetic methods in geophysics, Methods in Geochemistry and Geophysics, vol. 42, Elsevier, 2008

[2] N. Bowditch, "The American prwactical navigator", National Imagery and mapping agency, Bethesda, Maryland, pp. 81-112, 1995

[3] D. Gebre-Egziabher, G.H. Elkaim, J.D. Powell and B.W. Parkinson, "Calibration of Strapdown Magnetometers in Magnetic Field Domain", Journal of Aerospace Engineering, vol. 19, pp. 87-102, 2006

[4] J. F. Vasconcelos, G. Elkaim, C. Silvestre, P. Oliveira, and B. Cardeira, "A Geometric Approach to Strapdown Magnetometer Calibration in Sensor Frame", IFAC Workshop on Navigation, Guidance, and Control of Underwater Vehicles (NGCUV), Killaloe, Ireland, April 2008

[5] A. Sabatini, "Quaternion-based extended Kalman filter for determining orientation by inertial and magnetic sensing", IEEE Transactions on Biomedical Engineering, vol. 53, pp. 1346-1356, 2006

[6] V. Skvortzov, H.-K. Lee, S. Bang, and Y. Lee, "Application of Electronic Compass for Mobile Robot in an Indoor Environment", IEEE International Conference on Robotics and Automation, pp. 2963-2970, 2007

[7] S.-W. Liu,; Z.-N. Zhang and J. Hung, "A high accuracy magnetic heading system composed of fluxgate magnetometers and a microcomputer", Proceedings of the IEEE National Aerospace and Electronics Conference, vol. 1, pp. 148-152, 1989

[8] P. Ripka, "Magnetic Sensors and Magnetometers", Measurement Science and Technology, Artech House, 2001

[9] Geomagnetism Canadian Geomagnetic Reference Field (CGRF), http://gsc.nrcan.gc.ca/geomag/field/cgrf_e.php

[10] I. Markovsky, A. Kukush and S.V. Huffel, "Consistent least squares fitting of ellipsoids", Numerische Mathematik, vol. 98(1), pp. 177-194, 2004

[11] Q. Li, and J.G. Griffiths, "Least squares ellipsoid specific fitting", in Proceedings of Geometric Modeling and Processing, pp. 335-340, 2004.

[12] C. H. Smith, M.J. Caruso, R.W. Schneider and T. Bratland, " New Perspective on Magnetic Field Sensing", Sensors Mag., 1998

[13] A.W. Fitzgibbon; M. Pilu and R.B. Fisher, "Direct least-squares fitting of ellipses", in IEEE Transactions on Pattern Analysis and Machine Intelligence, vol. 21, pp. 476-480, 1999